Phase Behavior, Crystallization, and Hierarchical Nanostructures in Self-Organized Thermoset Blends of Epoxy Resin and Amphiphilic Poly(ethylene oxide)-*block*-poly(propylene oxide)-*block*-poly(ethylene oxide) Triblock Copolymers

Qipeng Guo,*,† Ralf Thomann, and Wolfram Gronski*

Institut für Makromolekulare Chemie, University of Freiburg, Stefan-Meier-Str. 31, 79104 Freiburg, Germany

Thomas Thurn-Albrecht

Fakultät für Physik, University of Freiburg, Hermann-Herder-Str. 3, 79104 Freiburg, Germany

Received November 13, 2001; Revised Manuscript Received January 29, 2002

ABSTRACT: Nanostructured thermoset blends of bisphenol A-type epoxy resin (ER) and amphiphilic poly(ethylene oxide)-*block*-poly(propylene oxide)-*block*-poly(ethylene oxide) (PEO−PPO−PEO) triblock copolymers were successfully prepared. Two samples of PEO−PPO−PEO triblock copolymer with different ethylene oxide (EO) contents, denoted as EO30 with 30 wt % EO content and EO80 with 80 wt % EO content, were used to form the self-organized thermoset blends of varying compositions using 4,4′-methylenedianiline (MDA) as curing agent. The phase behavior, crystallization, and morphology were investigated by differential scanning calorimetry (DSC), transmission electron microscopy (TEM), atomic force microscopy (AFM), and small-angle X-ray scattering (SAXS). It was found that macroscopic phase separation took place in the MDA-cured ER/EO30 blends containing 60−80 wt % EO30 triblock copolymer. The MDA-cured ER/EO30 blends with EO30 content up to 50 wt % do not show macroscopic phase separation but exhibit nanostructures on the order of 10−30 nm as revealed by both the TEM and SAXS studies. The AFM study further shows that the ER/EO30 blend at some composition displays structural inhomogeneity at two different nanoscales and is hierarchically nanostructured. The spherical PPO domains with an average size of about 10 nm are uniformly dispersed in the 80/20 ER/EO30 blend; meanwhile, a structural inhomogeneity on the order of 50−200 nm is observed. The ER/EO80 blends are not macroscopically phase-separated over the entire composition range because of the much higher PEO content of the EO80 triblock copolymer. However, the ER/EO80 blends show composition-dependent nanostructures on the order of 10−100 nm. The 80/20 ER/EO80 blend displays hierarchical structures at two different nanoscales, i.e., a bicontinuous microphase structure on the order of about 100 nm and spherical domains of 10−20 nm in diameter uniformly dispersed in both the continuous microphases. The blends with 60 wt % and higher EO80 content are completely volume-filled with spherulites. Bundles of PEO lamellae with spacing of 20−30 nm interwoven with a microphase structure on the order of about 100 nm are revealed by AFM study for the 30/70 ER/EO80 blend.

Introduction

Control of structure and morphology on the nanometer scale is becoming an increasingly important aspect of numerous technologies ranging from biomaterials to information systems. As size dimensions shrink, it is clear that the structure and architecture of these polymeric materials will become crucial. This significant reduction in size can produce dramatic changes in the behavior and properties of the materials. During the past decades, considerable attention has been paid to the design, preparation, and engineering of nanostructured materials for desired properties and functional purposes.[1−8] Particularly, there has been a great deal of interest in the preparation and characterization of nanostructured polymeric materials.[6−8] For example, self-organized nanostructures of various block copolymer architectures have been constructed.[9,10] The nanoscale structure formation in block copolymers takes place based on the repulsion between the covalently bonded blocks,[11] typically leading to spherical, cylindrical, lamellar, and gyroid phases. Self-organized nanostructures have also been obtained based on ionic interactions,[12] coordination bonds,[13] and hydrogen bonds[14−16] between the repulsive blocks, allowing also hierarchical order and functional materials.[17,18] In addition, blending block copolymers with thermoplastic homopolymers have been widely employed to prepare polymeric materials with various nanoscale structures.[10,19]

However, little has been published on creating nanoscale structures in blends of thermoset and block copolymers.[20−23] The control of the morphology, the long-range order, and the microstructure formation on the nanometer scale in thermoset blends have not been addressed until 1997.[20] Although there has been a large body of literature on the subject of toughening of thermosets by rubber and high-T_g thermoplastics, as well as by some block copolymers, the thermoset blends so obtained are generally phase-separated macroscopically. Hillmyer and co-workers[20,21] successfully introduced a method of creating nanostructured thermoset blends with an amphiphilic block copolymer. Nanoscale structures have been controllably produced in cured

† Present address: Department of Chemical Engineering and Materials Science, University of Minnesota, Minneapolis, MN 55455.

* To whom correspondence should be addressed.

10.1021/ma011971h CCC: $22.00
Published on Web 03/09/2002

blends of a diglycidyl ether of bisphenol A (DGEBA)-type epoxy resin with amphiphilic poly(ethylene oxide)-*block*-poly(ethyl ethylene) (PEO−PEE) and poly(ethylene oxide)-*block*-poly(ethylene-*alt*-propylene) (PEO−PEP) block copolymers. The epoxy resin that selectively mixes with the PEO block could swell the PEO domains in the block copolymers without dissolving the polyalkane blocks and thus lead to an ordered, nanostructured material via in situ curing of epoxy resin. Cross-linking of epoxy matrix without macroscopic phase separation of the block copolymers led to stable structures with nanoscopic features; the cured material exhibited an ordered core−shell morphology on 10−20 nm length scales. The miscibility of PEO block with the epoxy resins is an important mechanistic feature leading to the ordered morphology. The findings reported by Hillmyer and co-workers have provided an incentive to take a further look at nanostructured thermoset network/amphiphilic block copolymer blends. Mijovic et al.[22] have reported an interesting preliminary investigation on thermoset blends of DGEBA-type epoxy resin with poly(ethylene oxide)-*block*-poly(propylene oxide) (PEO−PPO) diblock copolymer and poly(ethylene oxide)-*block*-poly(propylene oxide)-*block*-poly(ethylene oxide) (PEO−PPO−PEO) triblock copolymer using dielectric relaxation spectroscopy and atomic force microscopy (AFM). They obtained nanostructured thermoset blends of epoxy resin with PEO−PPO diblock copolymer. In contrast, macroscopic phase separation was observed in thermoset blends of epoxy resin with PEO−PPO−PEO triblock copolymer. During the preparation of this paper, another example of self-organized thermoset blends based on novolac resin and poly(2-vinylpyridine)-*block*-poly(isoprene) appears.[23]

To explore new principles for creating structures of controlled length scales that would result in novel materials with distinct and unusual properties, a systematic investigation of preparation−morphology−property relationships in thermoset/amphiphilic block copolymer blend systems is necessary. In this study, we have successfully prepared nanostructured thermoset blends of DGEBA-type epoxy resin (ER) with amphiphilic PEO−PPO−PEO triblock copolymers by carefully choosing the curing condition. It should be pointed out that controlling the nanostructures of thermoset/block copolymer blend systems by curing conditions is of crucial importance for control of final mechanical properties of the resulted nanomaterials. Two samples of PEO−PPO−PEO triblock copolymers with different ethylene oxide contents, namely, EO30 with 30 wt % EO content and EO80 with 80 wt % EO content, are selected to form self-organized thermoset blends of varying compositions with DGEBA-type ER using 4,4′-methylenedianiline (MDA) as curing agent. The phase behavior, morphology, and hierarchical nanoscale structures in the cured materials are revealed by differential scanning calorimetry (DSC), transmission electron microscopy (TEM), AFM, and small-angle X-ray scattering (SAXS). Crystallization and the semicrystalline morphology in the nanostructured MDA-cured ER/PEO−PPO−PEO thermoset blends are also addressed.

Experimental Section

Materials and Preparation of Samples. Two samples of PEO−PPO−PEO triblock copolymer, namely, poly(ethylene glycol)-*block*-poly(propylene glycol)-*block*-poly(ethylene glycol), were purchased from Aldrich Chemical Co., Inc. The first PEO−PPO−PEO sample, with average $M_n = 5800$ and 30 wt % ethylene glycol, is denoted as EO30; the second, with average $M_n = 8400$ and 80 wt % ethylene glycol, is denoted as EO80. The uncured epoxy resin is diglycidyl ether of bisphenol A (DGEBA) (Epikote 828 LV, Shell Chemicals) with an epoxide equivalent weight of 185. 4,4′-Methylenedianiline (MDA) (Aldrich Chemical Co., Inc.) was used as curing agent. To prepare the MDA-cured ER/PEO−PPO−PEO blends, PEO−PPO−PEO (EO30 or EO80) was first dissolved in DGEBA with continuous stirring at 120 °C. The curing agent MDA was then added to the mixture at 100 °C with continuous stirring until a homogeneous ternary mixture was obtained. MDA was used in stoichiometric epoxide/amine ratios. The mixture was then immediately poured into an aluminum pan, degassed at 90 °C in a vacuum, cured at 80 °C for 8 h, and then postcured successively at 150 °C for 2 h and 175 °C for 1 h.

Differential Scanning Calorimetry (DSC). The calorimetric measurements were made on a Perkin-Elmer Pyris 1 differential scanning calorimeter in a dry nitrogen atmosphere. Indium and tin standards were used for calibration for low- and high-temperature regions, respectively. Samples of about 8 mg were placed in the DSC pan. All samples were first heated to 100 °C from −60 °C at a rate of 20 °C/min (first heating scan) and kept at that temperature for 2 min; subsequently, they were cooled at a rate of −20 °C/min to detect crystallization (cooling scan). Following the cooling scan, a second scan was conducted at the same heating rate as the first. The midpoint of the slope change of the heat capacity plot of the second heating scan was taken as the glass transition temperature (T_g). The crystallization temperature (T_c) was taken as the minimum of the exothermic peak, whereas the melting temperature (T_m) was taken as the maximum of the endothermic peak. The degree of crystallinity, X_c, was calculated by the following equations:

$$X_c(\text{blend}) = (\Delta H_f + \Delta H_c)/\Delta H_f^{\circ} \quad (1)$$

$$X_c(\text{copolymer}) = X_c(\text{blend})/W(\text{copolymer}) \quad (2)$$

where $\Delta H_f^{\circ} = 205$ J/g is the heat of fusion of 100% crystalline PEO,[24] W is the weight fraction, ΔH_f is the heat of fusion of the blend, and ΔH_c is the heat of crystallization during the same heating scan.

Optical Microscopy. The overall morphology of the blends was investigated by optical microscopy using a Zeiss Axioplan 2 apparatus. The samples were placed between a glass slide and a glass cover for observation.

Transmission Electron Microscopy (TEM). Samples were microtomed at −60 °C with a Leica EMFCS instrument equipped with a diamond knife. The resulting ultrathin sections of 80 nm thickness were picked up on copper grids and stained in the vapor of an aqueous solution of RuO_4. Stained samples were imaged in a LEO Omega 912 transmission electron microscope (TEM) with an accelerating voltage of 120 kV.

Atomic Force Microscopy (AFM). AFM experiments were performed with a Nanoscope III scanning probe microscope. The phase images were obtained by operating the instrument in the tapping mode under ambient conditions. Images were taken at the fundamental resonance frequency of the Si cantilevers which was typically around 300 kHz. Typical scan speeds during recording were 0.3−1 line/s using scan heads with a maximum range of 16 × 16 μm. The phase images represent the variations of relative phase shifts and are thus able to distinguish materials by their material properties. The flat surfaces of the blend samples used for examination were obtained by cutting with a Diatome diamond knife at −60 °C using a Leica EMFCS microtome.

Small-Angle X-ray Scattering (SAXS). The small-angle X-ray scattering (SAXS) experiments were performed with a Kratky compact camera (Anton Paar K.G., Graz, Austria) at room temperature. The Cu Kα radiation from a sealed X-ray tube was reflected from a graphite monochromator. The range of scattering vector $s = 2 \sin \theta/\lambda$, where $\lambda = 0.154$ nm is the wavelength and 2θ the scattering angle, was 0.01−0.3 nm^{-1}.

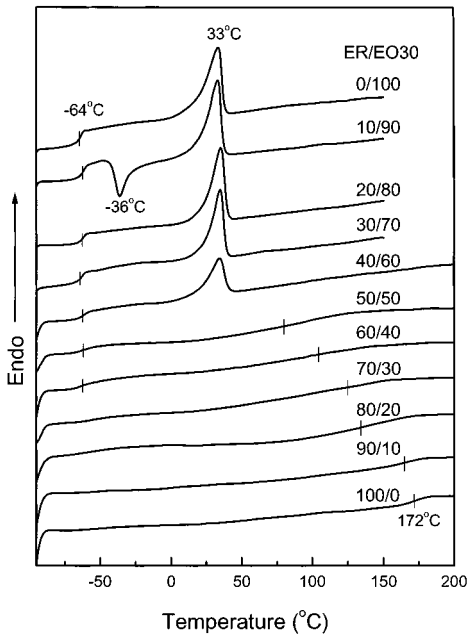

Figure 1. DSC thermograms of the second scan of the MDA-cured ER/EO30 blends after the cooling scan. The heating rate is 20 °C/min.

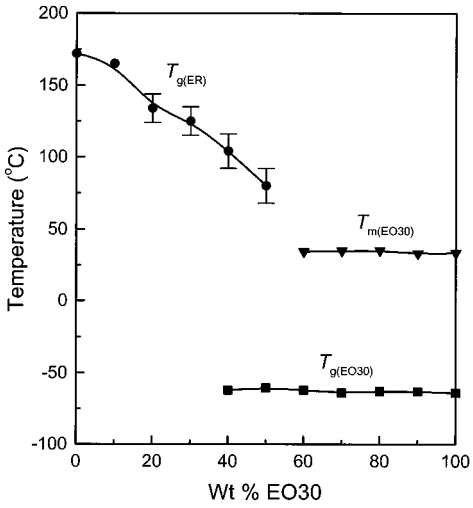

Figure 2. Thermal transitions of the second scan of the MDA-cured ER/EO30 blends.

The scattered intensity was recorded with a scintillation counter in a step-scanning mode. The sample of about 2 mm thickness was placed in a brass sample holder. The holder together with the collimation system was seated in an evacuated chamber. The background was corrected by subtraction of the scattering from an empty sample holder. The intensity was normalized to the incoming flux with the help of a moving slit device. The effect of the slitlike cross section of the beam was accounted for by desmearing the data using the standard procedure.[25]

Results and Discussion

Miscibility and Crystallization of MDA-Cured ER/EO30 Blends. Miscible blends containing a crystallizable component have attracted considerable interest. In contrast, little attention has been paid to miscible or even partially miscible blends of thermosetting resins with a crystallizable linear polymer.[26] From a consideration of thermodynamics, an increase in the molecular weight of either of the components of a miscible blend should reduce the entropy of mixing. Consequently,

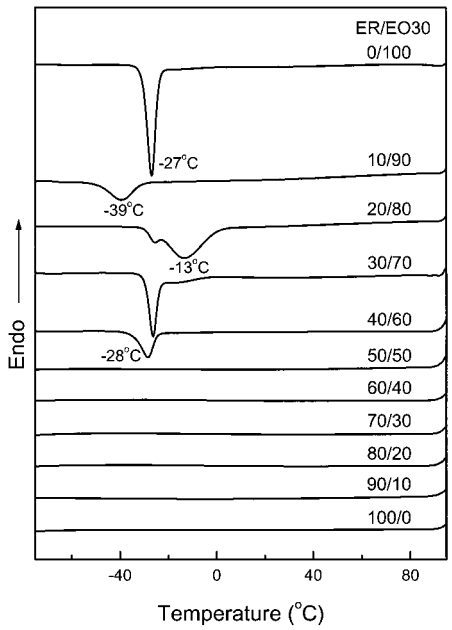

Figure 3. Crystallization curves of the MDA-cured ER/EO80 blends during the cooling at −20 °C/min.

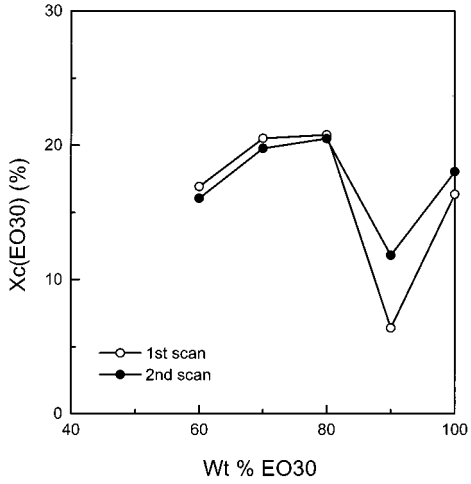

Figure 4. X_c(EO30) vs EO30 weight fraction of the MDA-cured ER/EO30 blends.

macroscopic phase separation induced by cross-linking is expected for systems with a positive (endothermic) enthalpy of mixing. Miscibility between the components has recently been observed only in a few cases for cross-linked blends with hydrogen-bonding interactions.[26] Thermoset blends of PEO homopolymer with several cured DGEBA-type ERs have been examined.[26−31] It has been shown that the miscibility of an ER with a linear polymer is very dependent on the nature of curing agent. PEO was found to be completely miscible with both DGEBA and aromatic diamine-cured ERs, including MDA-cured ER.[30,31]

All the MDA-cured ER/EO30 blends were clear after curing at 80 °C for 8 h. After postcuring for 2 h at 150 °C and 1 h at 175 °C, the blends containing 50 wt % or less EO30 triblock copolymer were still clear; the transparent solid samples were obtained. However, the blends containing 60−80 wt % EO30 triblock copolymer became cloudy or opaque after postcuring at 150 °C for 2 h. After the further postcuring for 1 h at 175 °C, the cloudy solid sample of the 40/60 ER/EO30 blend was obtained, whereas the 30/70 and 20/80 ER/EO30 blends

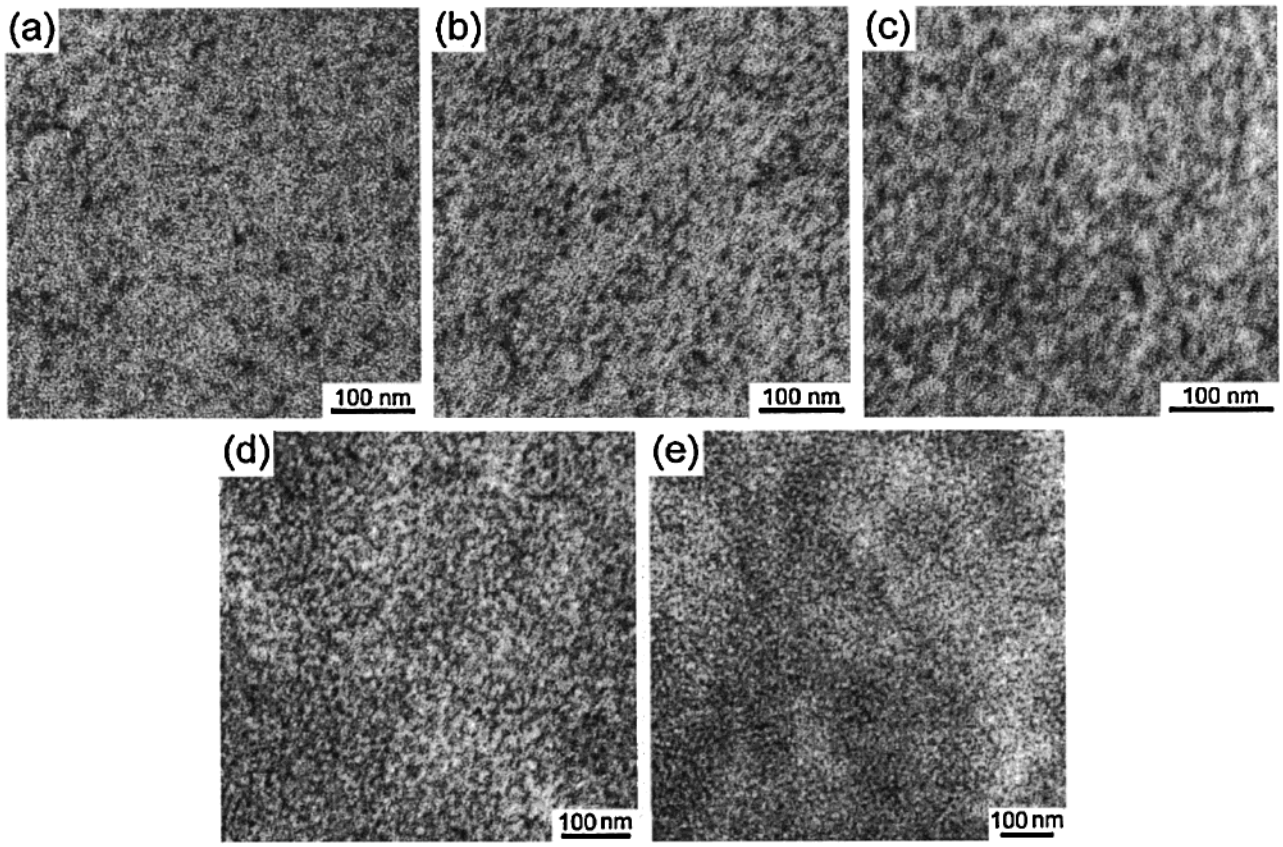

Figure 5. TEM micrographs of (a) 90/10, (b) 80/20, (c) 70/30, (d) 60/40, and (e) 50/50 MDA-cured ER/EO30 blends.

obtained appeared like white paste. The appearance of these three blends did not change at elevated temperatures. The 10/90 ER/EO30 blend after the postcuring was translucent at room temperature because of the slight crystallinity of the EO30 copolymer but became clear at the temperatures above the melting point of the EO30 copolymer (33 °C by DSC). These results suggest that macrophase separation took place in the cured blends containing 60−80 wt % EO30 triblock copolymer whereas the cured blends of all the other compositions were not phase-separated macroscopically.

The samples of all the MDA-cured ER/EO30 blends were subjected to DSC measurement. Figure 1 shows DSC thermogams of the second scan of the MDA-cured ER, EO30, and the MDA-cured ER/EO30 blends, and the results are summarized in Figure 2 as functions of blend composition. The EO30 triblock copolymer exhibits a glass transition, $T_{g(EO30)} = -64$ °C, and a melting point, $T_{m(EO30)} = 33$ °C, attributable to the amorphous PPO blocks and the crystalline PEO blocks, respectively. PEO is a semicrystalline polymer with a glass transition close to that of PPO and a melting point from 60 to 65 °C with a maximum crystallinity in excess of 80%.[32] PPO is an amorphous polymer with a glass transition ranging from −70 to −50 °C.[32] In the EO30 copolymer, the incorporation of PPO to PEO substantially hinders crystallization and reduces the melting point. The $T_{g(EO30)}$ is clearly observed in the ER/EO30 blends, and its value keeps almost unchanged with the EO30 content down to 40 wt %.

For the ER/EO30 blends with EO30 content up to 50 wt %, no melting peak is observed. DSC thermogams of the first scan (not shown here) also revealed that the as-prepared MDA-cured ER/EO30 blends with EO30 content up to 50 are amorphous. This implies that the PEO blocks of the EO30 copolymer are completely dissolved in the cured ER.

The MDA-cured ER displays a glass transition, $T_{g(ER)} = 172$ °C, which becomes very broad and ambiguous in the blends. $T_{g(ER)}$ shifts down to lower temperature with increasing EO30 content; its center reaches around 80 °C for the 50/50 ER/EO30 blend. It can be seen from Figure 2 that $T_{g(ER)}$ decreases rapidly with increasing EO30 content in the blends, indicating that the two components are miscible or at least partially miscible at these compositions. However, the reduction in T_g of the cured blends can result from a combination of two plasticization effects: internal and external. The dilution effect of the EO30 component can result in a reduction in cross-linking density of the network and hence a reduction in its T_g. The cross-linking density of the ER network decreases with increasing content of EO30. For the blends with low EO30 content, a three-dimensional cross-linking network structure forms. In contrast, for the blends with low ER content, only an imperfect network is formed, and there are highly branched ER chain molecules.

Figure 2 also contains the $T_{m(EO30)}$ values from the second scans as a function of the blend composition; they remain almost unaffected in the blends with EO30 content down to 50 wt %. This result is as expected for immiscible or partially miscible blends containing a crystallizable component.

For the pure EO30 copolymer and the blends containing 60−80 wt % EO30, no crystallization exotherm is observed during the heating since the crystallization of EO30 was sufficiently rapid to occur completely during the cooling scan. In contrast, the blend with 90 wt % EO30 shows a crystallization exotherm during heating above its T_g, indicating a more difficult crystallization

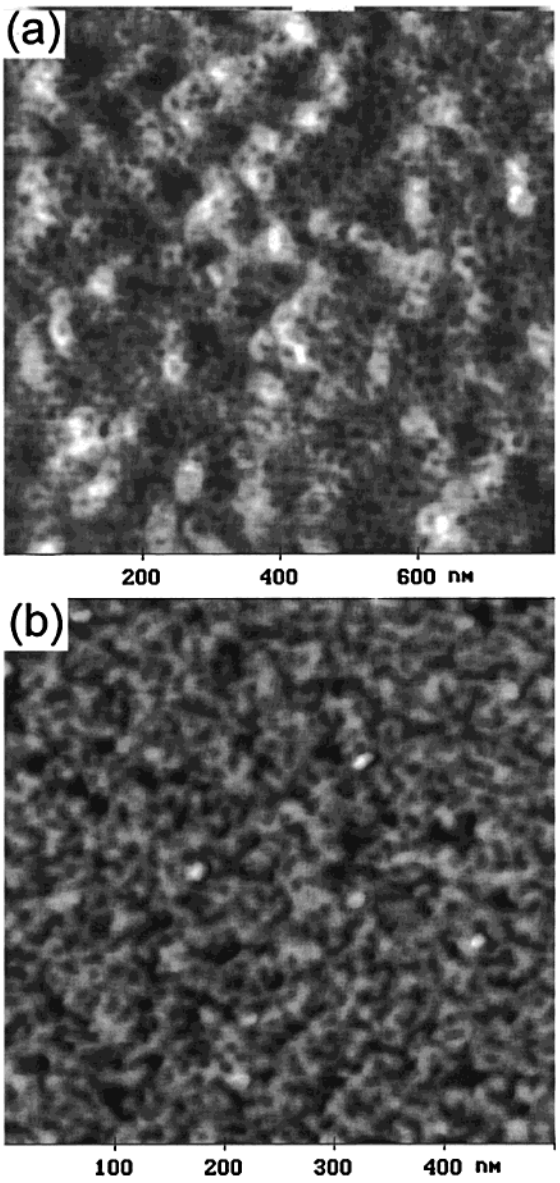

Figure 6. AFM phase images of (a) 80/20 and (b) 50/50 MDA-cured ER/EO30 blends.

of EO30 in this blend. The crystallization rate of EO30 in the 10/90 ER/EO30 blend is substantially decreased.

Figure 3 shows DSC thermograms of the cooling scan for the cured ER/EO30 blends at a cooling rate of 20 °C/min from 100 °C. The pure EO30 copolymer displays a crystallization peak at −27 °C, which remains at almost the same temperature in the blends containing 80−60 wt % EO30. This is characteristic of an immiscible blend. Furthermore, another crystallization peak appears at −13 °C for the blend containing 80 wt % EO30, indicating that the majority of crystallization was performed at an enhanced rate. This crystallization peak becomes a shoulder for the blend containing 70 wt % EO30. This phenomenon suggests that the ER-rich phase, which is separated out, can act as a nucleation agent in these blends. However, the crystallization peak shifts down to −39 °C for the blend containing 90 wt % EO30, indicating a reduced crystallization rate. This result supports the conclusion the blend containing 90 wt % EO30 is miscible in the melt. There is no crystallization exotherm during the cooling run for the blends containing 50 wt % or less EO30 copolymer, suggesting that these blends are miscible.

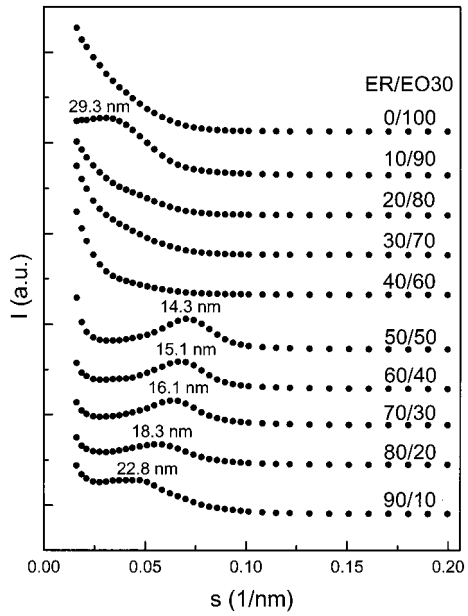

Figure 7. Desmeared SAXS patterns of MDA-cured ER/EO30 blends. The scattering vector $s = 2 \sin \theta/\lambda$. $\lambda = 0.154$ nm is the wavelength and 2θ the scattering angle.

The values of X_c(EO30) for the ER/EO30 blends are plotted as a function of blend composition in Figure 4. The pure EO30 copolymer shows a crystallinity, X_c-(EO30), less than 20%. The incorporation of amorphous PPO to PEO in the EO30 copolymer substantially hinders crystallization and greatly reduces its crystallinity. The X_c(EO30) values do not change considerably in the blends containing 80−60 wt % EO30. However, it is interesting to see that the X_c(EO30) shows a marked drop for the blend containing 90% EO30 copolymer owing to its miscibility.

It is interesting to compare the present results with those reported by Mijovic et al.[22] for the MDA-cured ER/PEO−PPO−PEO blends. The PEO−PPO−PEO triblock copolymer they used also contained 30 wt % ethylene glycol, but with a lower molecular weight ($M_n = 4400$) than EO30 ($M_n = 5800$). They observed macrophase separation for the 80/20 and 50/50 ER/PEO−PPO−PEO blends cured with MDA at 120 °C even though their triblock copolymer had a lower molecular weight. The triblock copolymer-containing blends were initially homogeneous and transparent; however, macrophase separation took place during curing at 120 °C, and the blend turned opaque. For the blend containing 20 wt % copolymer, spherical domains of copolymer with diameter of 10−50 μm were dispersed within the continuous ER phase. For the blend containing 50 wt % copolymer, the morphology observed was a combined one between the copolymer dispersed and the bicontinuous phase structures. The size of the phase structure was on the order of 50−100 μm.

The discrepancy of these two studies can be considered to be due to the different curing conditions. It has been proven that the phase behavior in thermoset blends of epoxy resin with a linear polymer strongly depends on the curing condition.[26] The phase behavior and morphology of a thermosetting polymer blend are determined by both thermodynamic and kinetic factors. For the blend in which one or both two components can cross-link, a semiinterpenetrating network (semi-IPN) or an interpenetrating network (IPN) may form. In this semi-IPN or IPN, the components which are initially

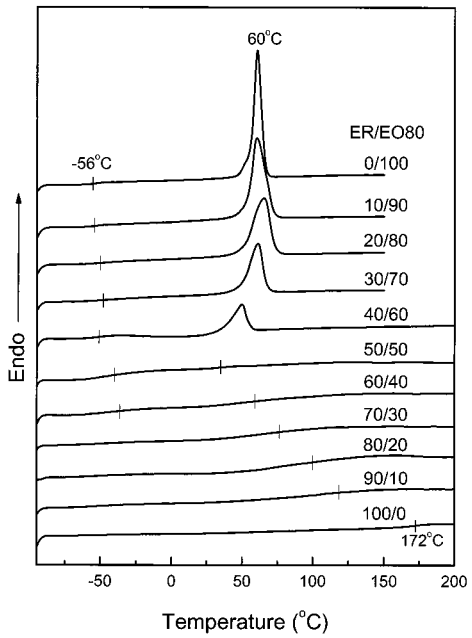

Figure 8. DSC thermograms of the second scan of the MDA-cured ER/EO80 blends after the cooling scan. The heating rate is 20 °C/min.

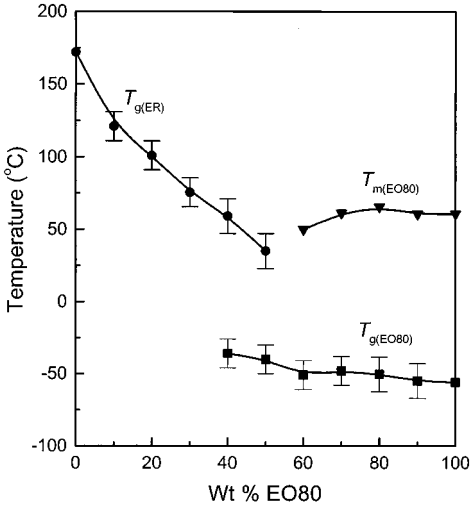

Figure 9. Thermal transitions of the second scan of the MDA-cured ER/EO80 blends.

immiscible may exhibit some characteristics of miscibility; i.e., the semi-IPN or IPN can be considered as a compatibilized immiscible polymer blend. On the other hand, the resulting increase in molecular weight causes a decrease in the configurational entropy of mixing as the cure proceeds. Therefore, curing may cause phase separation in an initial miscible blend. The phase separation process is governed not only by the thermodynamic factor but also by the kinetic factor. Raising the curing temperature increases the rate of the curing reaction and reduces the time for gelation. If gelation occurs prior to phase separation, no domains appear. On the other hand, raising the curing temperature enhances the mobility of molecule, so that phase separation occurs relatively easy. Curing reaction and phase separation are competitive. The macrophase-separated blends were obtained by Mijovic et al.[22] at an initial curing temperature of 120 °C, whereas no macrophase separation was observed in this study at an initial curing temperature of 80 °C. These results imply that

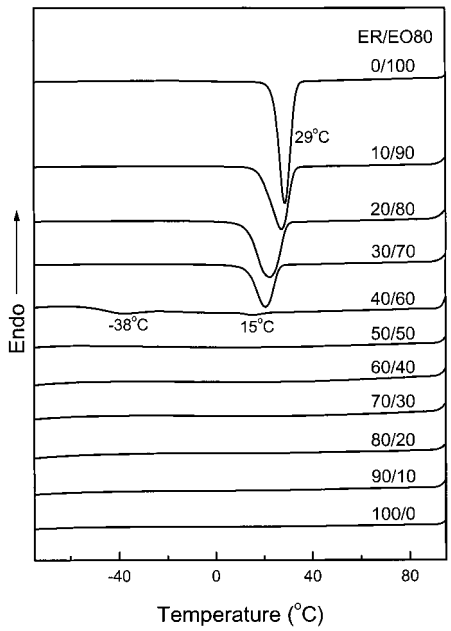

Figure 10. Crystallization curves of the MDA-cured ER/EO30 blends during the cooling at −20 °C/min.

the kinetic factor is dominant in this system, and elevating the curing temperature is more beneficial for phase separation.

Morphology and Hierarchical Nanostructures of MDA-Cured ER/EO30 Blends. The morphology of the cured ER/EO30 blends was investigated by TEM. The TEM micrographs of 90/10, 80/20, 70/30, 60/40, and 50/50 ER/EO30 blends are presented in Figure 5. The heterogeneous morphology at nanoscales is observed in all the cases. The dark areas are PPO microphases because the PPO block was preferentially stained with RuO_4 compared to the cured ER matrix.[33] For the 90/10 ER/EO30 blend, the PPO spherical domains (the dark areas) with an average size in diameter of about 10 nm are dispersed in a continuous cured ER matrix (Figure 5a). The TEM micrograph of 90/10 ER/EO30 blend clearly shows spherical micelles morphology. With increasing EO30 content, the morphology of the cured blends changes gradually. The 80/20 ER/EO30 blend gives rise to a similar morphology (Figure 5b). The spherical PPO micelles (the dark areas) with a size of about 10 nm are dispersed in the continuous ER-rich microphase.

When the EO30 content rises to 30 wt %, PPO microdomains are highly coagulated in a continuous ER-rich microphase (Figure 5c), forming wormlike micelles. The TEM micrograph of the 70/30 ER/EO30 blend exhibits some characteristic of a bicontinuous microphase structure. The size of the microphase structure was on the order of 10−30 nm. For the blend containing 40 wt % EO30, wormlike micelles are formed; the TEM micrograph exhibits a bicontinuous microphase structure (Figure 5d). The size of the microphase structure was on the order of 10−20 nm. A combined morphology of wormlike micelles and a bicontinuous microphase structure was observed in the blend containing 50 wt % EO30 (Figure 5e). This morphology will clearly be displayed by the further AFM study below.

Morphologies of the MDA-cured ER/EO30 blends were also studied by AFM. The AFM phase images of cured ER/EO30 blends clearly show microphase separation at nanoscales for various compositions (80/20, Figure 6a;

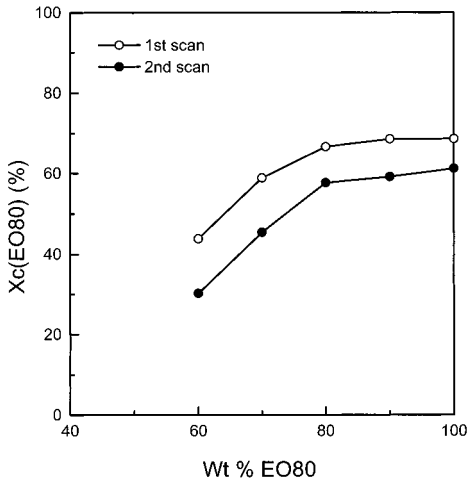

Figure 11. X_c(EO80) vs EO80 weight fraction of the MDA-cured ER/EO80 blends.

50/50, Figure 6b). The bright areas that are relatively stiff[34] are the ER-rich microphase composed of cross-linked ER network swollen with small amount of PEO blocks. The dark areas are the soft PPO domains shielded by coronae of PEO blocks. The gray areas contain insufficient cross-linked ER and more PEO blocks compared to the bright areas. It is interesting to notice that the 80/20 ER/EO30 blend exhibits hierarchical nanostructures. The dark PPO spherical domains with an average size in diameter of about 10 nm are well dispersed everywhere. This is in agreement with the TEM observation (Figure 5b). Furthermore, the AFM phase image (Figure 6a) reveals a structural inhomogeneity on the order of 50−200 nm. The 80/20 ER/EO30 blend displays structural inhomogeneity at two different nanoscales and is hierarchically nanostructured. The existence of structural inhomogeneity at two nanoscales can be accounted for by the evolution of the phase behavior during the curing process. The curing reaction between DGEBA and MDA resulted in the formation of cross-linked ER network swollen with a small amount of EO30 and then separated out to some extent to form an ER-rich phase with size of 50−200 nm from another phase composed of EO30 and insufficiently cured ER. This nanoscale phase separation caused the structural inhomogeneity on the order of 50−200 nm. Because of unfavorable interactions of PPO with the ER network as well as with the insufficiently cured ER, microphase separation took place within both the phases to form the PPO spherical domains with size on the order of 10 nm.

Figure 6b shows an AFM phase image of the 50/50 ER/EO30 blend. Both the spherical and wormlike PPO micelles (the black areas) are observed. The AFM phase image also clearly reveals characteristic of a bicontinuous microphase structure. The size of the microphase structure in the 50/50 ER/EO30 blend is on the order of 10−30 nm.

SAXS measurements have been performed at room temperature for samples of plain EO30 and ER/EO30 blends to characterize their microphase structures. Desmeared SAXS patterns for the EO30 and ER/EO30 blends are shown in Figure 7. For the plain EO30 triblock copolymer, no scattering peak is observed under the experimental conditions. However, a scattering peak is observed for the 10/90 ER/EO30 blend, corresponding to a long spacing of 29.3 nm in real space. Because the 10/90 ER/EO30 blend was miscible in the melt as shown by the DSC study, this result implies that the ER phase formed micelles in the EO30 matrix. The average

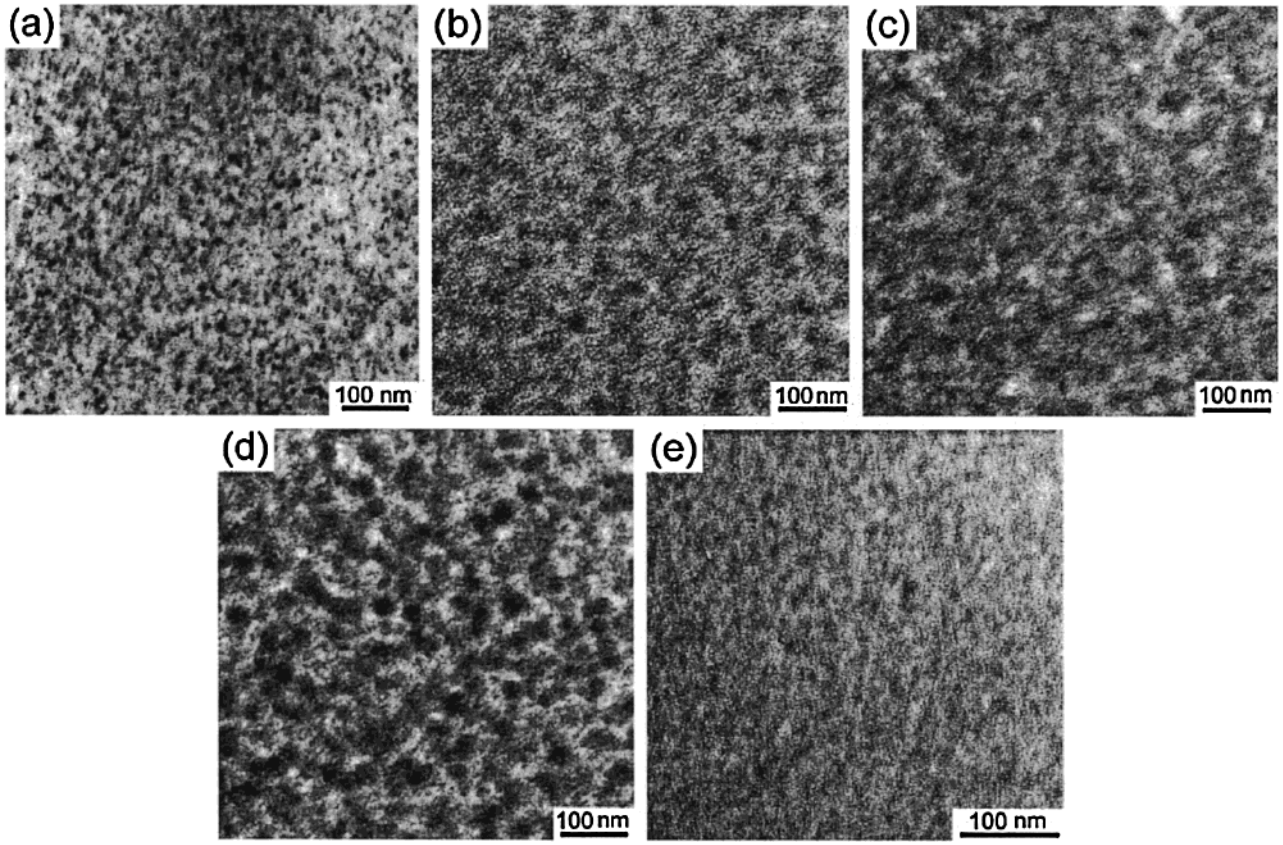

Figure 12. TEM micrographs of (a) 90/10, (b) 80/20, (c) 70/30, (d) 60/40, and (e) 50/50 MDA-cured ER/EO80 blends.

distance between the neighboring spherical micelles is 29.3 nm. This scattering peak becomes an ambiguous shoulder in the 20/80 and 30/70 ER/EO30 blends and disappears in the 40/60 ER/EO30 blends owing to the phase separation.

For the ER/EO30 blends containing 10−50 wt % EO30, a well-defined scattering peak is observed. With increasing EO30 content, the position of the scattering peak, i.e., the value of the scattering vector *s*, gradually increases, corresponding to a decrease of long spacing in real space from 22.8 to 14.3 nm as indicated in the figure. For the 90/10 and 80/20 ER/EO30 blends, these long spacing values are 22.8 and 18.3 nm, respectively, corresponding to the average distances between the neighboring spherical micelles. These results are in accordance with the TEM study (Figure 5a,b). For the ER/EO30 blends containing 30−50 wt % EO30, the long spacing values correspond to the average size of the microphase structure which decreases with increase of the EO30 content, agreeable with the TEM observation (Figure 5c−e).

Miscibility and Crystallization of MDA-Cured ER/EO80 Blends. The MDA-cured ER/EO80 blends with 60 wt % or higher EO80 were opaque at room temperature; this resulted from the crystallization of EO80 in the blends. All the blends were however transparent just above the melting point of EO80, indicating that EO80 and the cured ER are miscible in the molten state. The DSC thermograms of the second scan of the MDA-cured ER/EO80 blends are shown in Figure 8, and the results are presented in Figure 9 as functions of blend composition.

Figure 8 shows DSC thermogams of the second scan of the MDA-cured ER, EO80, and the MDA-cured ER/EO80 blends, and the results are summarized in Figure 9 as functions of blend composition. The EO80 triblock copolymer has a glass transition, $T_{g(EO80)} = -56$ °C, and a melting point, $T_{m(EO30)} = 60$ °C, attributable to the amorphous PPO blocks and the crystalline PEO blocks, respectively. $T_{g(EO80)}$ remains almost unchanged in the blends with ER content up to 60 wt %, corresponding to the PPO-rich microphase in these blends. Furthermore, the blends with EO80 content up to 50 wt % display a composition-dependent glass transition, $T_{g(ER)}$, as illustrated in Figure 9, indicative of an ER-rich microphase. No melting peak is observed for the ER/EO80 blends with EO80 content up to 50 wt %; DSC thermogams of the first scan (not shown here) also displayed that the as-prepared MDA-cured ER/EO80 blends of these compositions are amorphous. This result shows that the PEO blocks of the EO80 copolymer are completely dissolved in the cured ER-rich microphase.

Figure 9 shows that the $T_{g(ER)}$ of the blends decreases rapidly with increasing EO80 content. The reduction in $T_{g(ER)}$ of the ER-rich microphase can result from a combination of both the dilution effect of the PEO blocks of the EO80 component and the reduction in cross-linking density of the ER network.

Figure 9 also illustrates that the $T_{m(EO80)}$ in the blends tends to decrease with increasing ER content as expected. The T_m depression is a common phenomenon for miscible blends containing one crystallizable component.[35,36] However, morphological factors can also influence the $T_{m(EO80)}$.

The crystallization rate of PEO block in the cured ER/EO80 blends also decreases during cooling from the melt. Figure 10 shows DSC thermograms of the cooling scan for the cured ER/EO80 blends at a cooling rate of 20 °C/min from 100 °C. The crystallization peak shifts to lower temperatures with increasing ER content, and there is no crystallization exotherm during the cooling run for the blends containing less than 60 wt % EO80.

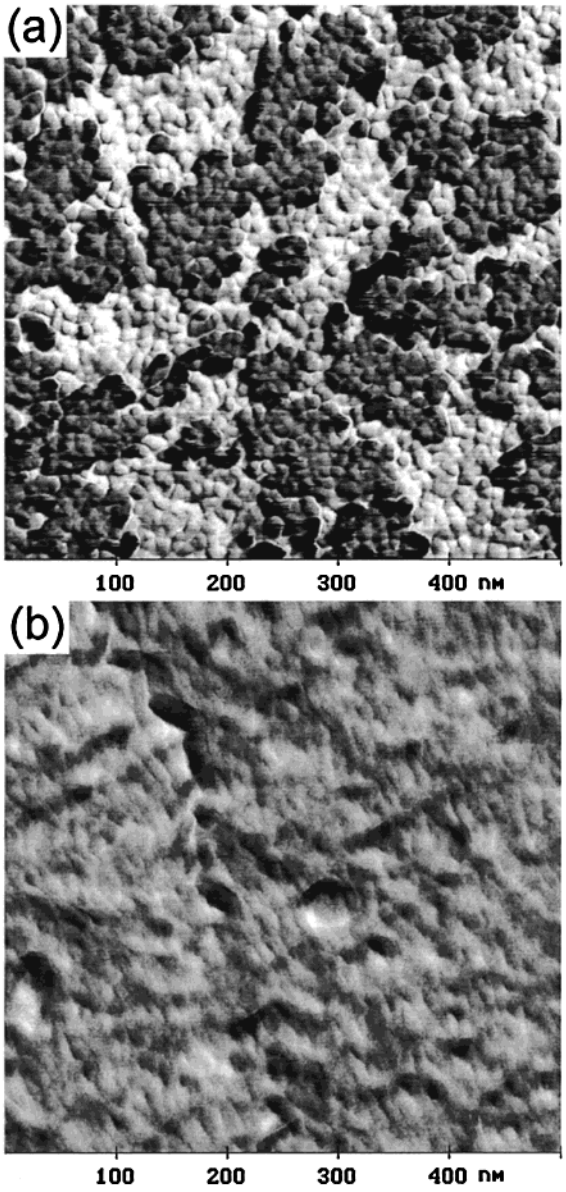

Figure 13. AFM phase images of (a) 80/20 and (b) 50/50 MDA-cured ER/EO80 blends.

The overall crystallization rate of PEO block of EO80 copolymer in the cured blends decreases substantially with increasing ER content, which can be ascribed to the much higher T_g of the MDA-cured ER (172 °C) compared to that of EO80 (−56 °C). Figure 10 illustrates that the 40/60 ER/EO80 blend displays another crystallization exotherm at −38 °C beyond the crystallization peak at 15 °C. It is known that PEO can crystallize by either heterogeneous or homogeneous nucleation.[37] The appearance of the two crystallization exotherms of the 40/60 ER/EO80 blend can be attributed to sequential heterogeneous and homogeneous nucleation. Initially, crystallization is induced by heterogeneous nucleation starting from 15 °C during the cooling scans. The crystallization rate of PEO block in the 40/60 ER/EO80 blend is very slow, and the number of heterogeneous

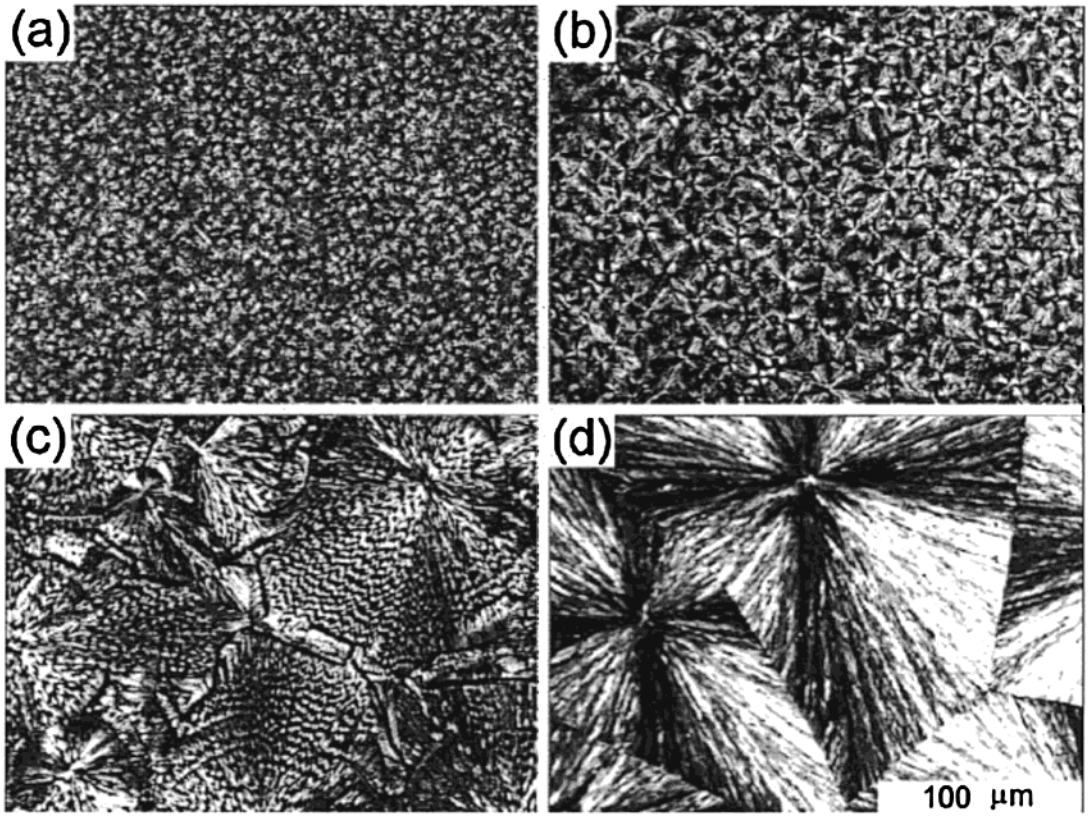

Figure 14. Optical micrographs of (a) 40/60, (b) 30/70, (c) 20/80, and (d) 0/100 MDA-cured ER/EO80 blends crystallized at 23 °C.

nuclei is small. Consequently, the crystallization process is not completed when the temperature reaches about −38 °C where homogeneous nucleation starts after formation of primary nuclei by the PEO block chains.

The values of X_c(EO80) for the ER/EO80 blends are plotted as a function of blend composition in Figure 11. The X_c(EO80) values for the first scan are all higher than those for the second scan. The crystallization of the as-prepared samples is much more complete than that of the second scan because of the long residence time at room temperature. However, for both the first and the second scans, the X_c(EO80) values gradually decrease with EO80 content down to 60 wt %.

The DSC results presented here clearly show that the ER/EO80 blends are not macroscopically phase-separated over the entire blend composition range. There exist however two microphases in the ER/EO80 blends. The PPO blocks form a separated microphase whereas the ER and the PEO blocks which are miscible form another microphase. The enhanced miscibility of the EO80 copolymer with the MDA-cured ER compared to the EO30 copolymer is because of the much higher PEO content of the EO80 copolymer.

Morphology and Hierarchical Nanostructures of MDA-Cured ER/EO80 Blends. The morphology of the cured ER/EO80 blends was also examined by TEM. Figure 12 shows the TEM micrographs of 90/10, 80/20, 70/30, 60/40, and 50/50 ER/EO80 blends. All of these blends display a heterogeneous morphology at nanoscales. For the 90/10 ER/EO80 blend, the PPO spherical domains (the dark areas) with an average size of about 10 nm are dispersed in a continuous cured ER matrix (Figure 12a). The TEM micrograph of 90/10 ER/EO80 blend also shows wormlike micelles morphology. The 90/10 ER/EO80 blend exhibits a combined morphology of both the spherical and wormlike micelles. With increasing EO80 content, PPO microdomains begin to coagulate and form wormlike micelles; the blends show characteristics of a bicontinuous microphase structure (Figure 12b−e). The size of the microphase structure is on the order of 50−100 nm for the blends containing 20−40 wt % EO80. However, the size of the microphase structure was substantially decreased for the 50/50 ER/EO80 blend, to the order of 10−30 nm.

Figure 13 shows AFM phase images of 80/20 and 50/50 ER/EO80 blends. The AFM phase images of the 80/20 ER/EO80 blend also reveals hierarchical nanostructures; the blend was microphase-separated at two different nanoscales (Figure 13a). First, the blend displays a bicontinuous microphase structure with size on the order of about 100 nm. The light areas are the ER-rich microphase and the dark areas the PPO-rich microphase. Second, spherical domains with size in diameter of 10−20 nm are uniformly dispersed in both the dark ER-rich microphase and the light PPO-rich microphase. The 80/20 ER/EO80 blend is hierarchically nanostructured, displaying structural inhomogeneity at two different nanoscales. The occurrence of structural inhomogeneity at two nanoscales can be explained by the evolution of the phase behavior during the curing process as discussed for the 80/20 ER/EO30 blend. Figure 13b presents an AFM phase images of the 50/50 ER/EO80 blend. The morphology of the blend shows characteristics of wormlike PPO micelles and a bicontinuous microphase structure. The AFM phase image also clearly reveals characteristics of a bicontinuous microphase structure. The size of the microphase structure in the 50/50 ER/EO80 blend is on the order of 10−30 nm, the same as observed by TEM (Figure 12e).

SAXS measurements were used to characterize the microphase structures of plain EO80 and of ER/EO80 blends. Unfortunately, desmeared SAXS patterns for

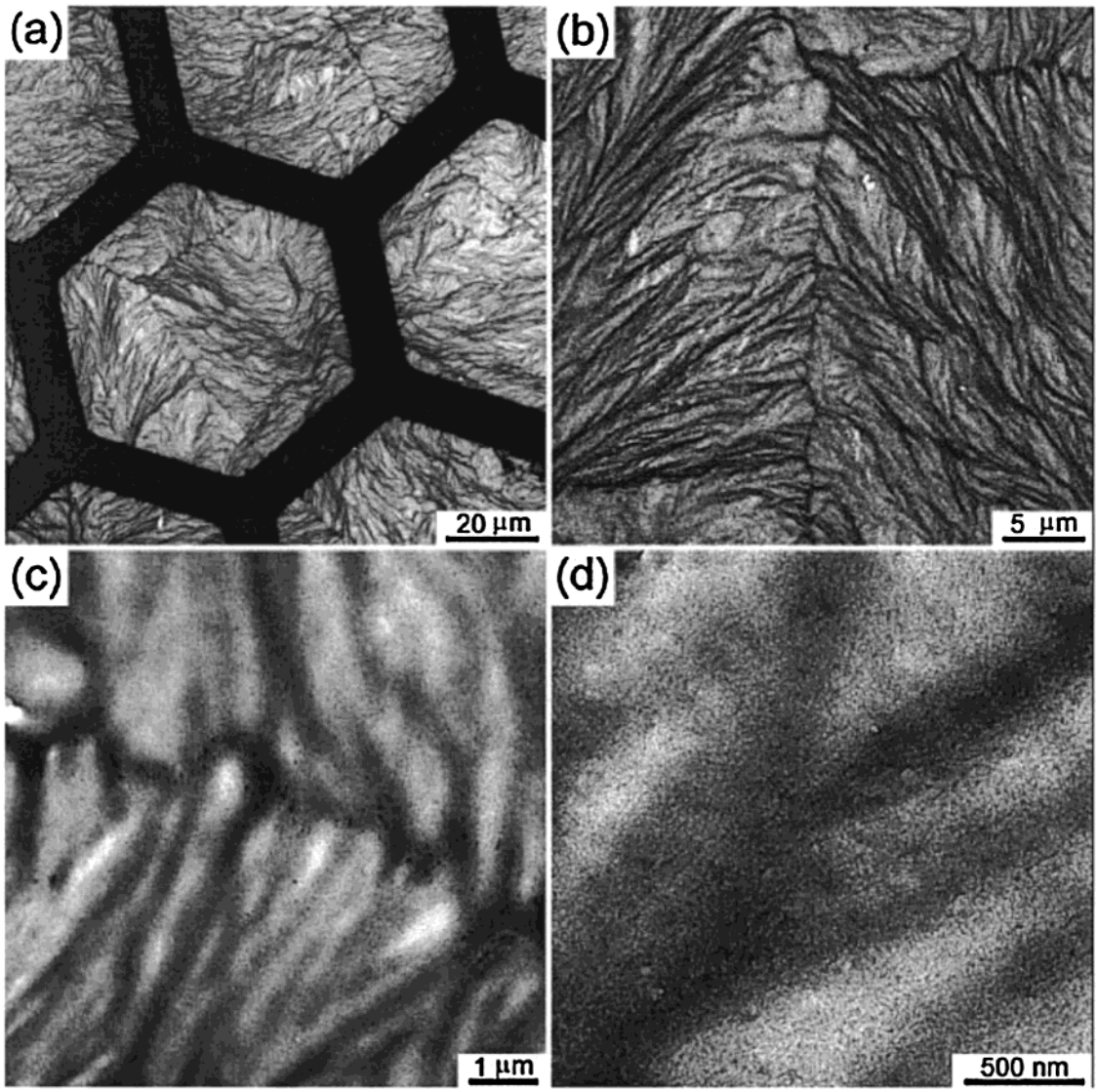

Figure 15. TEM micrographs of 30/70 MDA-cured ER/EO80 blend.

the ER/EO80 blends with EO80 content up to 50 wt % did not give any scattering peak. This is presumably because of the low electron contrast between the different microphases for these blends.

Spherulites were observed under a polarizing microscope in the cured ER/EO80 blends with ER content up to 40 wt %. Figure 14 shows the optical micrographs of these blends isothermally crystallized at 23 °C. The blends with EO80 content down to 60 wt % are still completely volume-filled with spherulites, but the size of the spherulites remarkably decreases with increasing ER content. The spherulitic morphology becomes more irregular or coarser. It is noted that the spherulites of 20/80 ER/EO80 blend (Figure 14c) are cracked, and the others are not. The occurrence of cracks is because of the volume shrinkage and the resulted negative pressure effect in a thicker film during the crystallization process.[28,38]

TEM and AFM were used to further examine the semicrystalline morphology of these blends. Figure 15 displays TEM micrographs of a 30/70 ER/EO80 blend at different magnifications. Figure 15a clearly shows that the 30/70 ER/EO80 blend is completely volume-filled with spherulites. The interspherulitic boundary is dark because it was composed of amorphous components which were preferentially stained with RuO_4. The spherulites appear rather coarse; the crystalline fibrils are clearly seen at higher magnifications (Figure 15b–d). The darker amorphous regions are also observed between the crystalline fibrils. It should be pointed out that, for the blends with EO80 content as high as 70 wt %, the curing reaction could hardly be completed owing to the diluent effect and only highly branched ER molecules formed. The amorphous cured ER molecules may segregate interfibrillarly, interlamellarly, and interspherulitically during the crystallization process of the PEO block.

Figure 16 shows an AFM phase image of the 30/70 ER/EO80 blend. The AFM phase image clearly shows bundles of PEO crystalline lamellae. The spacing of the PEO lamellae is 20–30 nm. In between, the blend displays a microphase structure of about 100 nm interwoven with the bundles of PEO crystalline lamellae.

It should be pointed out that the results presented here on the semicrystalline morphology are preliminary. The morphology of crystalline/amorphous block copolymers and their blends is very complicated.[39–42] A further detailed study is needed to completely understand the semicrystalline morphology and the segregation of the

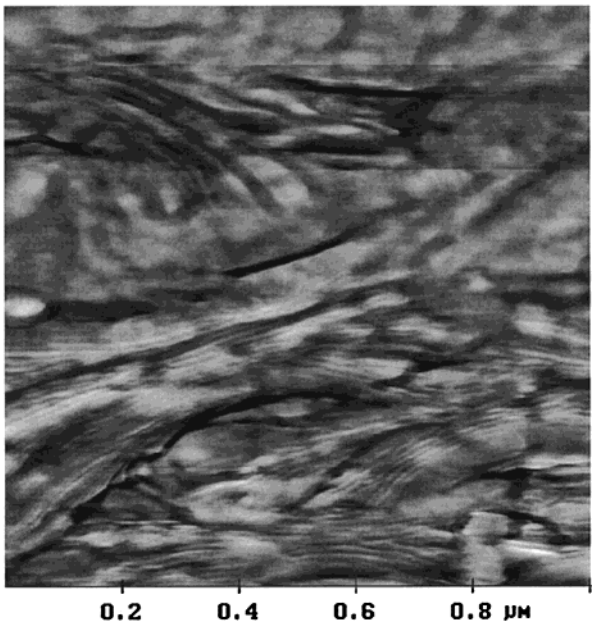

Figure 16. AFM phase image of 30/70 MDA-cured ER/EO80 blend.

cured ER in the nanostructured MDA-cured ER/EO80 thermoset blends.

Conclusions

We have successfully prepared nanostructured thermoset blends of bisphenol A-type ER and amphiphilic PEO−PPO−PEO triblock copolymers. Macroscopic phase separation took place in the MDA-cured ER/EO30 blends containing 60−80 wt % EO30 triblock copolymer. However, the nanostructures on the order of 10−30 nm are obtained for MDA-cured ER/EO30 blends with EO30 content up to 50 wt % which do not show macroscopic phase separation. The 80/20 ER/EO30 blend displays structural inhomogeneity at two different nanoscales and is hierarchically nanostructured. The spherical PPO domains with an average size of about 10 nm are uniformly dispersed; meanwhile, there exists a structural inhomogeneity on the order of 50−200 nm. The ER/EO80 blends are not macroscopically phase-separated over the entire composition range because of the much higher PEO content of the EO80 triblock copolymer but show composition-dependent nanostructures on the order of 10−100 nm. The nanostructured 80/20 ER/EO80 blend also displays hierarchical structures at two different nanoscales, i.e., a bicontinuous microphase structure on the order of about 100 nm and spherical domains of 10−20 nm in diameter uniformly dispersed in both the continuous microphases. The blends with 60 wt % and higher EO80 content are completely volume-filled with crystalline spherulites. Bundles of PEO lamellae with spacing of 20−30 nm are interwoven with a microphase structure on the order of about 100 nm. The results presented here have provided not only a clear physical picture on the phase behavior, morphology, and hierarchical nanoscale structures in self-organized ER/PEO−PPO−PEO thermoset/amphiphilic block copolymer blends but also a basic understanding on the preparation−morphology−property relationships in thermoset/amphiphilic block copolymer blend systems. We have also demonstrated by this study how to control the nanostructures of thermoset/block copolymer blend systems by optimizing the curing conditions, which is of crucial importance for control of final mechanical properties of this kind of novel nanomaterials.

Acknowledgment. The authors are indebted to Mrs. B. Heck for assistance in the SAXS measurements. Q.G. expresses his gratitude to the Alexander von Humboldt Foundation for awarding the prestigious Humboldt Research Fellowship.

References and Notes

(1) Ball, P. *Made to Measure: New Materials for the 21st Century*; Princeton University Press: Princeton, NJ, 1998.
(2) Whitesides, G. M.; Mathais, J. P.; Seto, C. *Science* **1991**, *254*, 1312.
(3) Martin, C. R. *Science* **1994**, *266*, 1961.
(4) Firouzi, A.; Kumar, D.; Bull, L. M.; Besier, T.; Sieger, P.; Huo, Q.; Walker, S. A.; Zasadzinski, J. A.; Glinka, C.; Nicol, J.; Margolese, D.; Stucky, G. D.; Chmelka, B. F. *Science* **1995**, *267*, 1138.
(5) Collins, P. G.; Zettl, A.; Bando, H.; Thess, A.; Smalley, R. E. *Science* **1997**, *278*, 100.
(6) Kalinina, O.; Kumacheva, E. *Macromolecules* **1999**, *32*, 4122.
(7) Giannelis, E. P.; Krishnamoorti, R.; Manias, E. *Adv. Polym. Sci.* **1999**, *138*, 107.
(8) Oriakhi, C. *Chem. Br.* **1998** (Nov), 59.
(9) Bates, F. S.; Fredrickson, G. H. *Annu. Rev. Phys. Chem.* **1990**, *41*, 525.
(10) Hamley, I. W. *The Physics of Block Copolymers;* Oxford University Press: Oxford, 1998.
(11) Muthukumar, M.; Ober, C. K.; Thomas, E. L. *Science* **1997**, *277*, 1225.
(12) Antonietti, M.; Conrad, J.; Thünemann, A. *Macromolecules* **1994**, *27*, 6007.
(13) Ruokolainen, J.; Tanner, J.; ten Brinke, G.; Ikkala, O.; Torkkeli, M.; Serimaa, R. *Macromolecules* **1995**, *28*, 7779.
(14) Ruokolainen, J.; ten Brinke, G.; Ikkala, O.; Torkkeli, M.; Serimaa, R. *Macromolecules* **1996**, *29*, 3409.
(15) Ruokolainen, J.; Tanner, J.; Ikkala, O.; ten Brinke, G.; Thomas, E. L. *Macromolecules* **1998**, *31*, 3532.
(16) Kosonen, H.; Ruokolainen, J.; Knaapila, M.; Torkkeli, M.; Jokela, K.; Serimaa, R.; ten Brinke, G.; Bras, W.; Monkman, A. P.; Ikkala, O. *Macromolecules* **2000**, *33*, 8671.
(17) Ruokolainen, J.; ten Brinke, G.; Ikkala, O. T. *Adv. Mater.* **1999**, *11*, 777.
(18) Ruokolainen, J.; Mäkinen, R.; Torkkeli, M.; Serimaa, R.; Mäkelä, T.; ten Brinke, G.; Ikkala, O. *Science* **1998**, *280*, 557.
(19) Winey, K. I.; Thomas, E. L.; Fetters, L. J. *Macromolecules* **1992**, *25*, 2645.
(20) Hillmyer, M. A.; Lipic, P. M.; Hajduk, D.; Almdal, K.; Bates, F. S. *J. Am. Chem. Soc.* **1997**, *119*, 2749.
(21) Lipic, P. M.; Bates, F. S.; Hillmyer, M. A. *J. Am. Chem. Soc.* **1998**, *120*, 8963.
(22) Mijovic, J.; Shen, M.; Sy, J. W.; Mondragon, I. *Macromolecules* **2000**, *33*, 5235.
(23) Kosonen, H.; Ruokolainen, J.; Nyholm, P.; Ikkala, O. *Macromolecules* **2001**, *34*, 3046.
(24) Vidotto, G.; Levy, D. L.; Kovacs, A. J. *Kolloid Z. Polym.* **1969**, *230*, 289.
(25) Strobl, G. *Acta Crystallogr.* **1970**, *A26*, 367.
(26) Guo, Q. In *Polymer Blends and Alloys*; Shonaike, G. O., Simon, G., Eds.; Marcel Dekker: New York, 1999; Chapter 6, pp 155−187.
(27) Guo, Q.; Peng, X.; Wang, Z. *Polym. Bull. (Berlin)* **1989**, *21*, 593.
(28) Guo, Q.; Peng, X.; Wang, Z. *Polymer* **1991**, *32*, 53.
(29) Luo, X.; Zheng, S.; Zhang, N.; Ma, D. *Polymer* **1994**, *35*, 2619.
(30) Zheng, S.; Zhang, N.; Luo, X.; Ma, D. *Polymer* **1995**, *36*, 3609.
(31) Guo, Q.; Harrats, C.; Groeninckx, G.; Koch, M. J. H. *Polymer* **2001**, *42*, 4127.
(32) Guo, Q.; Sun, K.; Fang, T.; Qi, Y.; Feng, Z. *J. Appl. Polym. Sci.* **1993**, *48*, 547.
(33) Trent, J. S.; Scheinbeim, J. I.; Couchman, P. R. *Macromolecules* **1983**, *16*, 589.
(34) Thomann, Y.; Thomann, R.; Bar, G.; Ganter, M.; Machutta, B.; Mülhaupt, R. *J. Microsc.* **1999**, *195*, 161.

(35) Nishi, T.; Wang, T. T. *Macromolecules* **1975**, *8*, 909.
(36) Imken, R. L.; Paul, D. R.; Barlow, J. W. *Polym. Eng. Sci.*. **1976**, *16*, 593.
(37) Wunderlich, B. *Macromolecular Physics;* Academic Press: New York, 1976; Vol. 2, p 24.
(38) Thomann, R.; Wang, C.; Kressler, J.; Mülhaupt, R. *Macromol. Chem. Phys.* **1996**, *197*, 1085.
(39) Hamley, I. W. *Adv. Polym. Sci.* **1999**, *148*, 113.
(40) Ryan, A. J.; Hamley, I. W.; Bras, W.; Bates. F. S. *Macromolecules* **1995**, *28*, 3860.
(41) Hong, S.; Yang, L.; MacKnight, W. J.; Gido, S. P. *Macromolecules* **2001**, *34*, 7009.
(42) Kim, G.; Han, C. C.; Libera, M.; Jackson, C. L. *Macromolecules* **2001**, *34*, 7336.

MA011971H